Journal of
Computational and Theoretical Nanoscience
Vol. 2, 75–87, 2005

Surface-Plasmon Coupled Nonequilibrium Thermoelectric Refrigerators and Power Generators

Ronggui Yang, Arvind Narayanaswamy, and Gang Chen*

Mechanical Engineering Department, Massachusetts Institute Technology, Cambridge, MA 02139, USA

RESEARCH ARTICLE

Thermoelectric energy conversion devices rely on electron transport for energy conversion, while phonon heat conduction is usually detrimental for the energy conversion efficiency. Higher energy conversion efficiency is possible if the electrons and phonons can be decoupled. This paper proposes and investigates surface-plasmon coupled nonequilibrium thermoelectric devices. In such devices, the energy transport from the heat source of a power generator or the cooling target of a refrigerator to the thermoelectric element is limited to electrons through the coupling of surface-plasmons across a vacuum gap of the order of tens of nanometers. In the power generation mode, this method of thermal-energy coupling allows the creation of hot electrons in the thermoelectric element. In the refrigeration mode, cold electrons created in the thermoelectric element can be coupled to the cooling target through the surface-plasmons. Under certain conditions, these surface-plasmon coupled nonequilibrium thermoelectric devices perform significantly better than conventional thermoelectric devices based on the same materials.

Keywords: Surface Plasmon, Thermoelectrics, Nonequilibrium, Refrigerator, Power Generator.

1. INTRODUCTION

Direct energy conversion between heat and electricity using thermoelectric effects such as the Seebeck for power generation and the Peltier effect for refrigeration has been studied extensively.[1,2] In a thermoelectric device, three competing processes occur simultaneously: the useful Peltier effect or Seebeck effect, the volumetric Joule heating, and the heat conduction from the hot end to the cold end. Device analysis shows that the performance of thermoelectric devices is determined by the materials figure of merit, $Z = S^2\sigma/k$, where S is the Seebeck coefficient, σ is the electrical conductivity, and k is the thermal conductivity. The thermal conductivity has contributions from both electrons and phonons. That is, $k = k_e + k_p$, where k_e and k_p are electron and phonon thermal conductivities respectively. Most research in thermoelectrics has focused on improving the figure of merit, and significantly progress has been made in the past decade.[2–4] In addition to the materials development, there are also new opportunities to create novel thermoelectric devices that can potentially outperform conventional thermoelectric devices. Different device configurations have been explored in the past. Past studies include the investigation of thermoelectric effects in pn junctions and minority carrier effects,[5,6] multistage thermoelectric devices,[7] and transient effects.[8] Recent examples are thermionic refrigeration and power generation based on single and multilayer structures.[9,10]

In thermoelectric devices it is the electrons that do the useful energy conversion work and the electron temperature that matters for energy conversion efficiency. Following the rationale of reducing the phonon thermal conductivity, if there is a way to impart energy to electrons only (by cutting off the energy transport through phonons between the heat source or the cooling target and the thermoelectric element) while minimizing the energy coupling between electrons and phonons, it is possible to obtain better performance of thermoelectric devices. Existing examples are the vacuum thermionic power generators[11] and electron tunneling refrigerators.[12] Electron thermionic emission, however, is limited by the work function of available materials, and electron tunneling requires extremely small gaps, of the order of several angstroms. An alternative way to decouple electrons

*Author to whom correspondence should be addressed.

 1546-198X/2005/2/075/013/$17.00+.25 doi:10.1166/jctn.2005.005

and phonons is to explore thermal radiation between two surfaces, for example, using photons to transfer the energy from the heat source to electrons in the power generation unit. Along this line, the most apparent way of utilizing such an effect is to use a thermophotovoltaic converter[13] in which photovoltaic cells convert the energy of the photons emitted by a thermal source into useful electrical energy. Thermophotovoltaics, however, is limited to photons with energy above the bandgap. If radiation can create sufficient non-equilibrium between electrons and phonons in a thermoelectric power generator or refrigerator the performance of such devices can be significantly improved. It has been long recognized that the nonequilibrium between electrons and phonons in the thermoelectric element can be exploited to improve the thermoelectric energy conversion efficiency,[14–18] but there exist no easy ways to create such nonequilibrium states between electrons and phonons to benefit from hot electrons for power generation or to benefit from the cold electrons for refrigeration. Taking power generation as an example, to take advantage of nonequilibrium between electrons and phonons, a small thermal radiation resistance is needed (1) to provide high energy flux to compensate the electron energy loss to phonons and thus create the nonequilibrium state of electrons and phonons (2) to reduce the temperature drop between the heat source and electrons in the thermoelectric element. The heat flux through far-field thermal radiation is generally too small to create nonequilibrium between electrons and phonons. Recent work on phonon–polariton coupling in the near-field shows that a heat flux as high as 10's or 100's W/cm^2 can be obtained when two half-spaces of polar semiconductor (such as silicon carbide or boron nitride) are separated by a nanoscale vacuum gap for a temperature difference of 10's K between the two surfaces.[19] We anticipate that near-field energy transfer due to surface-plasmons will have a similar behavior with the additional advantage that only electrons (or plasmons) participate in the energy exchange.

In this study, we develop models to investigate the potential of surface-plasmon coupled nonequilibrium thermoelectric refrigerators and power generators. This paper is organized as follows. In Section 2, we develop models for surface-plasmon-coupled nonequilibrium thermoelectric devices, including surface-plasmon energy transport model across a nanoscale vacuum gap and nonequilibrium electron–phonon energy transport model in the thermoelectric device, followed by discussion on material property selection criteria. Section 3 presents the calculation results for refrigerators and power generators followed by a brief summary in Section 4.

2. THEORETICAL MODEL

Figure 1(a) and (b) illustrates schematically a surface-plasmon coupled nonequilibrium thermoelectric refrigerator and power generator, respectively. A nanoscale vacuum

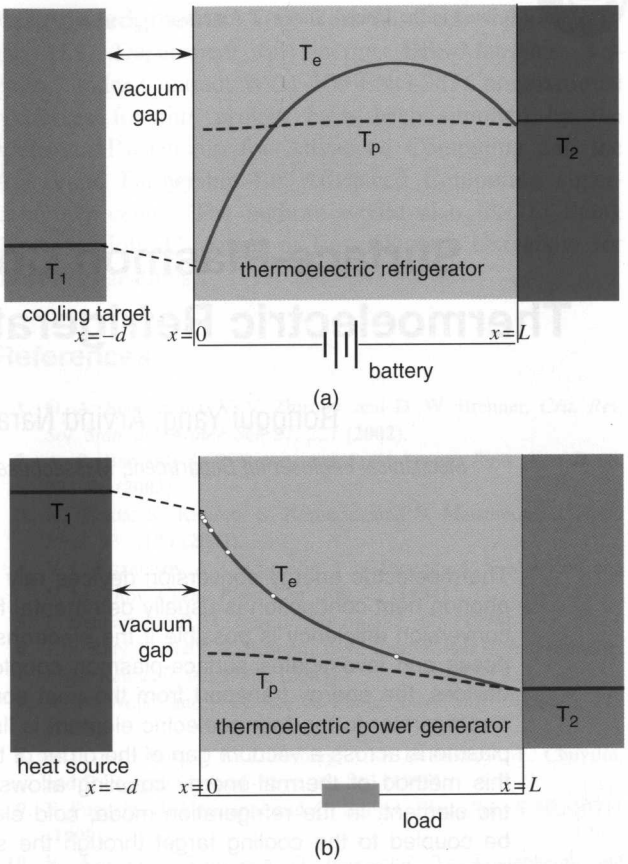

Fig. 1. Schematic drawing of surface-plasmon coupled nonequilibrium thermoelectric devices: (a) refrigerator, and (b) power generator. A nanoscale vacuum gap is to avoid the direct contact of the heat source or the cooling target from thermoelectric device, and thus cut-off the heat flow through phonons between the heat source or the cooling target and the thermoelectric device.

is present to avoid the direct contact of heat source or cooling target from thermoelectric element, and thus cutting-off the heat flow through phonons between the heat source or the cooling target and the thermoelectric element. The vacuum gap should range from a few nanometers to a few tens of nanometers to ensure high radiative energy flux. The cooling target or heat source should support surface plasmon polaritons or be coated with a thin film of a material that can support surface plasmon polaritons. Similarly, the side of the thermoelectric element facing the cooling target or heat source should also be coated with a thin film of the same material. Having the same material on both sides of the vacuum gap results in the largest energy transfer due to surface plasmons. Also illustrated in the figure are the typical electron and phonon temperature distributions in the devices, which will be justified subsequently. We will first present the surface-plasmon energy transport model in Section 2.1, and couple it to a nonequilibrium electron–phonon transport model for the whole device in Section 2.2. We will also develop criteria for good device performance. Section 2.3 outlines the material property selection rules.

2.1. Surface-Plasmon Energy Transport Model

Radiative energy transfer between two surfaces separated by more than a few characteristic wavelengths, as given by Wien's displacement law, is too small to create significant non-equilibrium effects between electrons and phonons in the thermoelectric element for our proposed application. Tunneling of normal evanescent waves can give rise to an enhancement in the radiative energy transfer, with a maximum radiative flux proportional to n^2 times of that of the blackbody flux in vacuum, where n is the material refractive index.[20,21] Although the possibility of utilizing this enhancement for thermophotovoltaic energy conversion has been studied theoretically as well as experimentally,[22,23] the increase in heat flux is still not sufficient for the current application. On the other hand, it has been found recently that excitation of electromagnetic surface waves, such as surface phonon–polaritons, can lead to an enhancement of radiative flux orders of magnitude higher than that of the blackbody limit.[24] The possibility of utilizing this effect for thermophotovoltaic energy conversion has been analyzed theoretically using materials that support surface phonon–polaritons. Similar enhancement of energy transfer can be achieved due to near-field coupling between surface plasmon polaritons, which involve electrons as opposed to phonons.

The radiative energy transfer between the heat source (or cooling target) and the thermoelectric element by surface plasmons is modeled following the same method used to model energy transfer between two half-spaces due to surface phonon–polaritons, using a combination of dyadic Green's function technique[25] and the fluctuation-dissipation theorem to characterize the spectral strength of the thermal sources.[26] Doped semiconductors with high electron or hole mobilities can support surface plasmon waves. A n-type semiconductor with the following dielectric function is assumed

$$\varepsilon(\omega)=\varepsilon_\infty-(\varepsilon_{DC}-\varepsilon_\infty)\left(\frac{\omega_{TO}^2}{\omega^2-\omega_{TO}^2+i\omega\gamma_p}\right)-\frac{\omega_p^2}{\omega(\omega+i\gamma_e)} \quad (1)$$

The first term on the right hand side of Eq. (1) is due to atomic polarization, the second term is due to the optical phonons, and the third term is due to the conduction electrons. We choose parameters that are close to that of InSb, with $\varepsilon_\infty=15.24$, $\varepsilon_{DC}=17.76$, $\omega_{TO}=0.022$ eV, $\gamma_p=3.56\times10^{-4}$ eV.[27] The plasma frequency is related to the doping by the relation

$$\omega_p^2=\frac{ne^2}{m_{eff}\varepsilon_0} \quad (2)$$

where n is the electron concentration, m_{eff} is the effective mass of the electrons, and ε_0 is the electrical permittivity of free space. The effect of doping on the radiative transfer is to vary the plasma frequency, ω_p, and the damping, γ_e. Though the entire device could be complicated, the heat source (or cooling target) and the thermoelectric element are modeled as two half-spaces that have the same plasmon frequency as shown in Figure 2(a). For comparison, the spectral "absorptivity" of a 10 nm thin film of InSb adjacent to a half-space of InSb is shown in Figure 3. The emitter is a half-space of InSb. Almost the entire energy incident on the thin film in the spectral range corresponding to transfer by plasmons is absorbed in this very thin layer. As long the major part of radiative energy transfer is due to surface plasmon polaritons, the exact configuration of the thermoelectric device can be approximated by that of two half-spaces separated by a vacuum layer since the penetration depth of surface plasmons is only around 10 nm. The spectral flux transfer between two half-spaces of InSb, with $\omega_p=0.18$ eV and $\gamma_e=5.33$ meV, at 400 K and 390 K with a vacuum gap in-between them is shown in Figure 4. The two peaks in the figure correspond to resonances due to surface waves. The smaller peak, which occurs around the surface phonon–polariton frequency, is due to the surface phonon polariton and the main peak, which occurs around the surface plasmon polariton frequency, is due to the surface plasmon of the conduction electrons. For our application, only radiative transfer by surface plasmons is desired. By doping InSb appropriately, the fraction of energy transfer due to phonons can be reduced. To do so, the surface plasmon polariton frequency would have to be sufficiently separated from the surface phonon polariton frequency. In addition, the optimum plasma frequency is also determined by the temperatures involved. Figure 5 shows the net energy transfer from one half-space at a constant temperature as a function of temperature difference between the two half-spaces. For comparison, the net energy transfer between two blackbodies, one of them at 500 K, is also shown in the same figure. The resonance effect of surface plasmon results in an energy transfer around 4 orders of magnitude higher than the far-field value. The net surface plasmon energy transfer is also a function of the distance between hot and cold surface (as shown in Fig. 4). The smaller the vacuum gap d, the larger is the energy transport flux with given temperature difference. The total energy flux due to

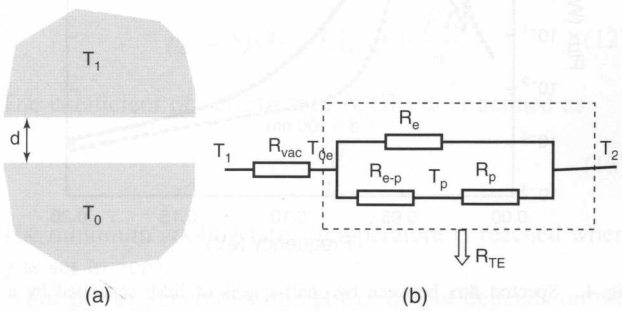

Fig. 2. (a) Schematic of half-spaces of InSb separated by a vacuum gap of thickness d, (b) thermal resistance network of the surface-plasmon coupled nonequilibrium devices.

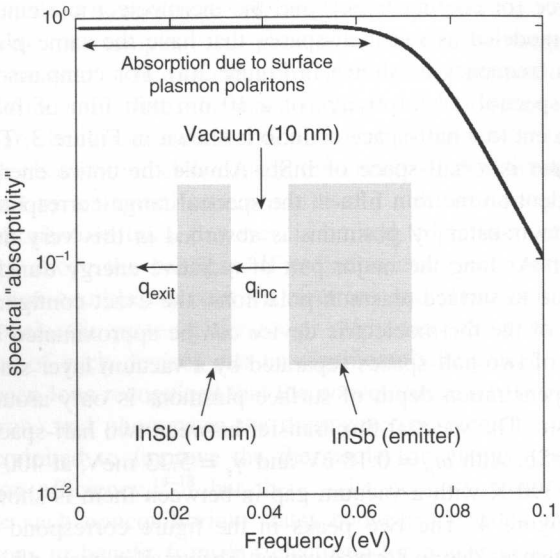

Fig. 3. Spectral "absorptivity" 10 nm film of InSb separated from a InSb half space (emitter) by a 10 nm layer of vacuum. "Absorptivity" is defined as the ratio $(q_{inc} - q_{exit})/q_{inc}$. This figure shows that only 10 nm of InSb is necessary to absorb all the surface plasmon energy flux. It confirms that our approximation of treating the thermoelectric device as two half-spaces of InSb separated by a 10 nm layer of vacuum is valid.

excitation of surface waves is proportional to $1/d^2$. In the rest of this paper, 10 nm vacuum is assumed.

2.2. Surface-Plasmon Coupled Nonequilibrium Thermoelectric Devices

Standard thermoelectric device models assume that electrons and phonons are under local equilibrium. However, depending on the electron–phonon energy exchange rate and the rate of heat input, the electrons can be heated

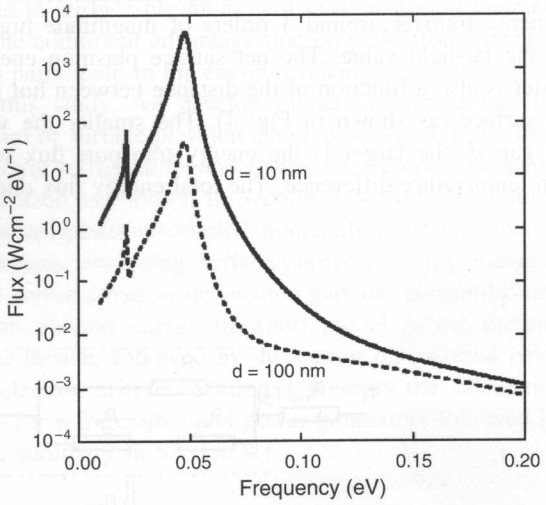

Fig. 4. Spectral flux between two half-spaces of InSb separated by a vacuum gap of thickness $d = 10$ nm and $d = 100$ nm. The plasma frequency is assumed to be 0.18 eV. The smaller peak corresponds to resonance due to surface phonon polaritons and the bigger peak corresponds to resonance due to surface plasmon polaritons.

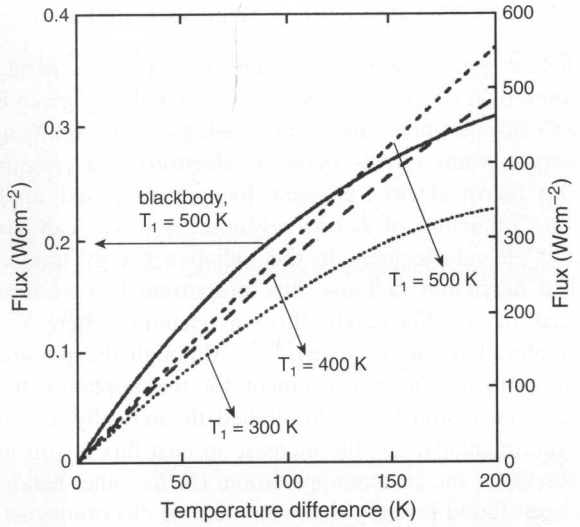

Fig. 5. Total energy transfer between two half-spaces of InSb. The hotter half-space is maintained at T_1 and the temperature of the colder half-space is varied. The x-axis is the temperature difference between the hot and cold bodies. The blackbody energy transfer, the hotter half-space maintained at 500 K, corresponds to the y-axis on the left. The other curves correspond to the y-axis on the right.

(or cooled) to a much higher (or lower) temperature than the phonons. Such a nonequilibrium electron–phonon effect, which is often called hot electron effect in high field electronics since electrical fields heat up electrons first, have been extensively studied for high field electronics[28–30] and laser-material interactions where the electrons can be thrown out of equilibrium from lattice due to excitation by ultra-short laser pulse.[31,32] A few papers have also dealt with nonequilibrium electron and phonon transport in thermoelectric research.[14–18] We follow an established way to deal with such a nonequilibrium situation, the two-temperature model, which assumes that electron and phonons are in equilibrium with their respective subsystems and have their own temperature, and that the boundary conditions can be separately formulated. For this treatment to be valid, the electron–electron collisions which randomize the electron energy should be frequent enough, a condition usually satisfied if the electron concentration is 10^{16} cm^{-3} or higher, as is the case in good thermoelectric materials. We further restricted our analysis to monopolar (single carrier) semiconductors and assumed that there is no electron-hole pair generated and thus no additional recombination heat needs to be considered. We also neglected the temperature dependence of thermoelectric properties (k_e, k_p, σ and S), thus no Thompson effect is included in the model. Under these approximations, the governing transport equations for electron and phonon subsystems in the thermoelectric element are:

$$k_e \frac{d^2T_e}{dx^2} - G(T_e - T_p) + \frac{j^2}{\sigma} = 0 \tag{3}$$

$$k_p \frac{d^2T_p}{dx^2} + G(T_e - T_p) = 0 \tag{4}$$

where T_e and T_p are electron and phonon temperatures respectively, j is the current density pass through the thermoelectric element, and G is the volumetric electron–phonon energy coupling constant, which can also be viewed as the cooling or heating rate of electrons due to their interaction with phonons. The first terms in Eqs. (3) and (4) are heat conduction terms due to electron carriers and phonon carriers respectively, $G(T_e - T_p)$ describes the energy coupling or interaction between electron and phonon subsystems, and $\frac{j^2}{\sigma}$ is the energy input to the electron subsystem due to Joule heating.

The general solutions for the electron and phonon temperatures are,

$$T_e(x) - T_p(x) = \theta_0 + \theta(x) \tag{5}$$

$$T_p(x) = -\frac{k_e}{k_e + k_p}\theta(x) - \frac{j^2}{2\sigma(k_e + k_p)}x^2 + C_3 x + C_4 \tag{6}$$

where

$$\theta_0 = \frac{j^2 k_p}{G\sigma(k_e + k_p)}, \quad \theta(x) = C_1 e^{mx} + C_2 e^{-mx} \tag{7}$$

and

$$m^2 = \frac{G(k_e + k_p)}{k_e k_p} \tag{8}$$

The above general solutions have been obtained before together with different boundary conditions to determine coefficients C_1 to C_4. The concept of coupling through surface plasmons requires us to establish new boundary conditions that are difficult to realize in conventional device configurations. If we look at the time scale, the characteristic time scale of creating a surface polariton mode is ω_p^{-1}, which in this case is $\approx$23 fs. Electron–electron scattering time is also around tens of femto-seconds. Finally, the characteristic time for energy transfer between electrons and phonons is given by the electron–phonon coupling constant, which can range from a pico-second to nano-seconds at low temperatures. Hence, this paper assumes that the surface polaritons are regenerated almost instantaneously. The radiative energy due to surface polaritons is first transferred to the electrons, which form a subsystem at the electron temperature, and finally to the phonons, which form another subsystem at the phonon or lattice temperature, through electron–phonon coupling. This scale analysis justifies the boundary conditions established below for the nonequilibrium thermoelectric devices. Although the temperature profiles seem different in the surface plasmon thermoelectric refrigerators [Fig. 1(a)] and power generators [Fig. 1(b)]. The boundary conditions for the control equations are actually similar.

At $x = L$, away from the plasmon coupling surfaces, we assume that the electrons and phonons are in equilibrium with each other at T_2. That is,

$$T_e = T_2 \quad \text{and} \quad T_p = T_2 \tag{9}$$

At $x = 0$, the phonon subsystem is assumed to be isolated, i.e.

$$\frac{dT_p}{dx} = 0. \tag{10}$$

This assumption is used in most of the calculation results presented in this paper except Figure 11 shown later, since the surface-plasmon energy transport calculation in Figure 4 shows that less than 10% of total energy coupling between the surfaces is through phonons and this percentage can be further reduced by appropriate doping to control the separation between frequencies of the surface plasmon and surface phonon–polariton.

The boundary condition for electron subsystem at $x = 0$ can be written as

$$q = SjT_e|_{x=0} - k_e \frac{dT_e}{dx}\bigg|_{x=0} \tag{11}$$

The first term is the Peltier cooling term, which represents the heat absorbed from the hot surface of the power generator or cold surface of the refrigerator. The second term is the heat conducted by electrons.

It is through q in Eq. (11) that we couple the equations of nonequilibrium electron–phonon transport model in thermoelectric devices to the surface-plasmon energy transport model across the vacuum. Because of this coupling, neither the heat flux nor the temperature at $x = 0$ (the interface between the vacuum and the thermoelectric element) are known variables. For power generators, the heat source temperature T_1 at $x = -d$ is usually taken as the input for efficiency calculation, where d is the size of the vacuum gap. For refrigerators, either the cooling target temperature T_1 or cooling power density is given for the performance calculation. Thus numerical iteration is inherently needed for the calculation of temperature distribution. After the temperature inside the thermoelectric element is known, we can determine the performance of the whole device.

To evaluate the refrigerator performance, the temperature at the interface of the vacuum and thermoelectric element can be calculated for a given cooling load (cooling rate) at a cooling target temperature T_1. Then the energy expenditure p_{in} for cooling can be written as

$$p_{\text{in}} = Sj(T_2 - T_e|_{x=0}) + \frac{j^2 L}{\sigma} \tag{12}$$

The coefficient of performance (COP) ϕ is defined as

$$\phi = \frac{q}{p_{\text{in}}} \tag{13}$$

The minimum cooling target temperature is reached when q is set to zero.

For power generators, the power output depends on the external electrical load resistance R_L. Often the external resistance is written as $R_L = \mu R_{\text{in}} = \mu(L/\sigma A)$, where μ is the electrical resistance ratio, R_{in} is the electrical resistance

RESEARCH ARTICLE

of the thermoelectric element and A is the cross-section area of the thermoelectric element. Then the electric current density in power generator can be written as

$$j = \frac{V_s}{R_{\mathrm{TOT}}A} = \frac{S(T_e|_{x=0} - T_2)}{(L/\sigma A + R_L)A} = \frac{S\sigma(T_e|_{x=0} - T_2)}{L(1+\mu)} \quad (14)$$

The power output p_0 is thus,

$$p_0 = \frac{j^2 R_L}{A} = \frac{S^2\sigma(T_e|_{x=0} - T_2)^2}{L}\frac{\mu}{(1+\mu)^2} = \frac{kZ(T_e|_{x=0} - T_2)^2}{L}\frac{\mu}{(1+\mu)^2} \quad (15)$$

The energy conversion efficiency η can be calculated as

$$\eta = \frac{p_0}{q} \quad (16)$$

We will also compare the COP and minimum temperature for refrigeration and the efficiency for power generation thus obtained with that of standard devices, for which the corresponding expressions are well documented.

We note that there are no simple equations for performance evaluation of surface-plasmon coupled nonequilibrium thermoelectric devices. The numerical simulations are carried out to obtain various optimum values. Before presenting any numerical results, however, we will develop some criteria that serve as guidelines for device design and materials selection.

From the above discussion, we see that in the proposed devices, an additional temperature drop between the heating (cooling) source and the thermoelectric element develops across the vacuum gap. We define an effective thermal resistance for the vacuum gap, R_{vac}, due to the surface-plasmon energy transport, where $R_{\mathrm{vac}} = (T_1 - T_e|_{x=0})/q$. This resistance must be small such that most temperature drop happens in the thermoelectric element rather than the vacuum gap, i.e.,

$$R_{\mathrm{vac}} \ll R_{\mathrm{TE}} \quad (17)$$

where R_{TE} is the total thermal resistance of the thermoelectric element, which will be determined next.

For conventional thermoelectric devices (both power generator and refrigerator), the thermal resistance is given by L/k. In the nonequilibrium thermoelectric devices, a first order analysis (neglecting the joule heating effect on thermal resistance model) gives the thermal resistance network as shown in Figure 2(b). When the energy is coupled from the heat source or the cooling object to the interface between the vacuum and the thermoelectric element, it is transported through two channels in the thermoelectric element. One is through the electron subsystem and the other is through the electron–phonon interaction and then the phonon subsystem. The electron–phonon coupling thermal resistance can be written as

$$R_{e-p} = \frac{1}{GL_{e-p}} \quad (18)$$

where L_{e-p} is the length over which electron and phonon subsystems has distinguishable temperatures. L_{e-p} is the thermoelectric element length or the electron cooling length, whichever is smaller. The electron cooling length l is defined as the distance required for electrons and phonons to reach equilibrium from the boundary where electrons is heated or cooled,[15, 17]

$$\frac{1}{l^2} = G\left[\frac{1}{k_e} + \frac{1}{k_p}\right] \quad (19)$$

The total thermal resistance of the thermoelectric element operating in nonequilibrium can be thus be approximated as,

$$R_{\mathrm{TE}} = \left(\frac{1}{R_e} + \frac{1}{R_{e-p} + R_p}\right)^{-1} = \left[\left(\frac{1}{GL_{e-p}} + \frac{L}{k_p}\right)^{-1} + \frac{k_e}{L}\right]^{-1} \quad (20)$$

If $(1/GL_{e-p})$ is much less than L/k_p, the nonequilibrium effect is not noticeable and Eq. (20) can be simplified to that of a conventional thermoelectric device, L/k. Thus, to have distinguishable benefit, R_{TE} must be larger than the thermal resistance of a conventional device, that is

$$R_{\mathrm{TE}} > \frac{L}{k} \quad (21)$$

In the other hand, when $(1/GL_{e-p} + L/k_p) \to \infty$, the thermoelectric element can be viewed as an almost perfect one with thermal conductivity of k_e and corresponding $Z = S^2\sigma/k_e$.

Thus one will apparently benefit from nonequilibrium electron–phonon effect, if

$$\frac{1}{GL_{e-p}} + \frac{L}{k_p} > \frac{L}{k_e}. \quad (22)$$

Normally k_p is larger than k_e for thermoelectric materials, then the criterion can be written as

$$\frac{1}{GL_{e-p}} > \frac{L}{k_e} \quad (23)$$

We note that in nanostructured thermoelectric materials, k_p is often reduced to the same order of magnitude as k_e. In such a case, Eq. (22) should be used as a criterion.

In summary, surface-plasmon nonequilibrium device will have superior performance than a conventional one when:

(1) $R_{\mathrm{vac}} \ll R_{\mathrm{TE}}$ to reduce the additional temperature drop due to surface-plasmon energy transfer. This criterion also explains why the coupling by conventional far field radiation or the tunneling of regular evanescent waves is not sufficient for the proposed device configurations.

(2) $1/GL_{e-p} > L/k_e$ to have distinguishable contribution from nonequilibrium electron–phonon temperatures.

2.3. Material Property Selection

The efficiency of conventional thermoelectric devices is determined by ZT. Reviews of past and current research in thermoelectrics should be consulted for progresses made.[1,2,33] Generally a good thermoelectric material has $S \sim 200\ \mu$V/K, $\sigma \sim 10^5\ \Omega^{-1}\,m^{-1}$. For the proposed devices, the electron–phonon coupling constant G is of crucial importance, as well as the plasmon frequency. The electron–phonon interaction is an active research area due to its important role in solid state physics, notably as the process that determine the electrical resistance, superconductivity, and the equilibrium dynamics of hot electrons. More often, the electron–phonon energy exchange is presented by electron energy relaxation time τ_e in literature.[28,30,34–37] Neglecting the electron kinetic energy, the electron–phonon coupling constant can be written as

$$G = \frac{3nk_B}{2\tau_e} \tag{24}$$

Clearly, G is proportional to the doping concentration in Eq. (24) and is a very complicated function of both the electron and phonon temperatures rather than a constant since τ_e depending on both the electron scattering mechanism and the degeneracy. References [35] and [36] summarize the theoretical form of τ_e for various scattering mechanisms and reference [38] for low dimensional systems. However, the theoretical value agrees only qualitatively with experimental results. A number of different techniques, including electrical transport (steady state) and optical methods (dynamics) have been used to study the electron energy relaxation.[29,30,38] Table I lists some experimental data of the energy relaxation time for various materials (after [29]). Clearly τ_e ranges from $0.1 \sim 10$ ps at room temperature. At low temperatures, τ_e can be as long as tens nanoseconds. Depending on the optimum doping concentration for optimum ZT, G ranges from 10^9 to 10^{13} W/(m^3 K). The optimum doping concentration for thermoelectric material varies from 10^{15} cm^{-3} or 10^{16} cm^{-3} for narrow bandgap materials (InSb[39], $Hg_{1-x}Cd_xTe$[40]) to 10^{19} cm^{-3} or 10^{20} cm^{-3} for wide bandgap materials (SiGe). Most good thermoelectric semiconductors have a G value around 10^{10} or 10^{12} W/(m^3 K) at their optimum ZT values. Metals have very high G, which is around $10^{16} \sim 10^{17}$ W/(m^3 K).[41]

In Russian literature,[14,15,17] the electron–phonon energy coupling constant is often given as electron cooling length. The electron–phonon cooling lengths l vary from 100's nanometers to several microns at room temperature. However it does not give the details about doping concentration dependence.

In our calculation, we used $S = 200\ \mu$V K^{-1}, $\sigma = 10^5\ \Omega^{-1}\,m^{-1}$ and $k = 2.0$ Wm^{-1}K^{-1}. G and k_e/k vary in different cases. With such material properties, the minimum temperature the cold end of a conventional thermoelectric refrigerator can achieve is 241 K at zero cooling load and a hot side temperature of 300 K. When this material is used to make a conventional thermoelectric power generator operating at 500 K to 300 K, the maximum efficiency is 7.03%.

Table I. Experimental data of the energy relaxation time (after Ref. 29).

Material	Lattice temperature (K)	Electron temperature (K)	τ_e (10^{-12} sec)
Si	8	29	110.0
		107	24.0
		222	2.94
		505	0.5
	77	107	23.0
		222	2.6
		505	0.43
	300	330	2.6
		505	0.37
Ge	100	100	27.0
	150	150	10.0
	200	200	6.0
	300	300	6.0
		400	6.0
		640	9.7
		1500	19.0
InSb	4.2	5	2×10^5
		10	3×10^5
		15	4×10^5
	1.15	1–15	$2.35–3.3 \times 10^5$
	20	20	5×10^5
	25	25	1.3×10^5
	77	77	
		122	1.76
		192	2.46
		297	3.37
GaAs	50	50	17.3
	80	80	1.7
	77	150	0.35
		300	0.65
		700	0.82
		1000	1.02
	300	350	1.42
		500	1.28
		800	1.94
		1000	1.88

3. RESULTS AND DISCUSSIONS

The model described in Section 2 has an inherent assumption that the electrons and phonons are well in equilibrium with each other in the heat source or cooling target while maintaining their nonequilibrium state in the thermoelectric element. This assumption can be justified through careful design of the surface of the heat source or cooling target. We can think of that the heat source or cooling target are made of a very thin surface plasmon material (such as InSb), coated on a metal layer. The high electron–phonon coupling constant of metal, which is usually around 5 orders of magnitude larger than that of semiconductors, ensures that the equilibrium between electrons and phonons in the metal underneath the material layer

that supports surface plasmon. Then the thickness of the surface plasmon supporting material must satisfy two conditions: (1) The thickness is large enough to support all the surface plasmon energy flux. As discussed in Figure 3, it should be more than 10 nm. (2) The electron and phonon temperature drop inside the surface plasmon material layer should be small. Figure 6(a) shows the temperature drop in the surface plasmon supporting layer under a cooling heat flux of $q = 50$ W/cm^2. Figure 6(a) shows the electron temperature drop $(T_e - T_m)$ and phonon temperature drop $(T_p - T_m)$ inside the surface plasmon supporting material layer, where T_m is the temperature at the surface of metal layer and surface plasmon material. Figure 6(b) shows the temperature drop at the plasmon material surface as a function of the thickness of surface-plasmon material.

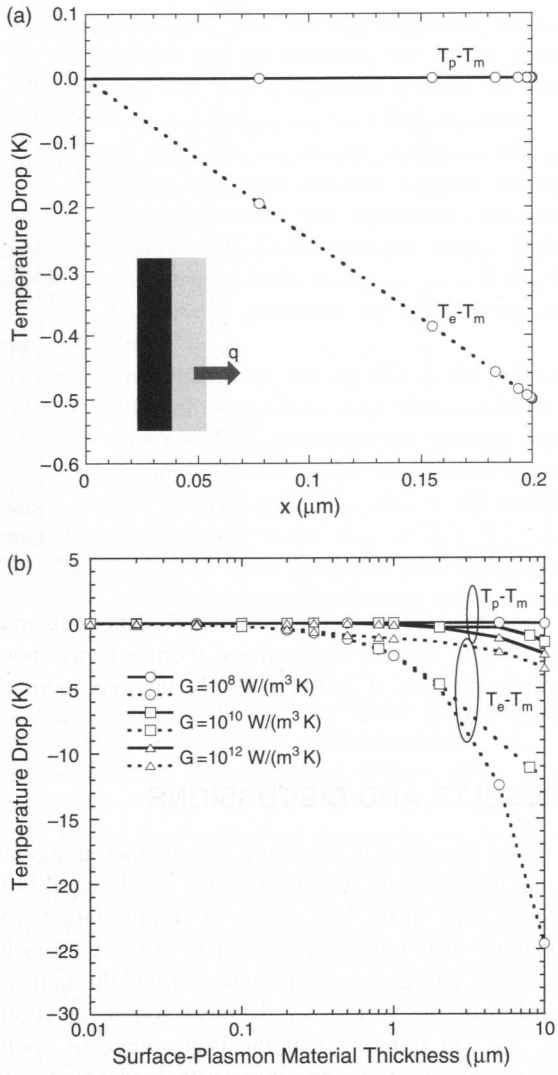

Fig. 6. The temperature drop in the surface plamson supporting layer with a thin metal layer underneath under a cooling heat flux of $q =$ 50 W/cm^2: (a) the electron $(T_e - T_m)$ and phonon $(T_p - T_m)$ temperature drop inside the surface plasmon supporting material layer, and (b) the temperature drop at the plasmon material surface as a function of the thickness of surface-plasmon material.

The smaller the electron–phonon coupling constant, the larger the electron temperature drop. The temperature drop is less than 2.5 K if the thickness of the surface plasmon material is less than 1 μm. Thus we can assume that the electron temperature and phonon temperature are in equilibrium and they are the same as cooling target or heat source temperature if the cooling target or heat source are coated with tens or several hundred nanometers of surface plasmon material with a thin metal layer underneath. In the rest, we present the calculation results for both surface plasmon coupled nonequilibrium refrigerators and power generators.

3.1. Refrigerator

Figure 7 shows the variation of several characteristic temperatures as a function of the current density under a cooling load of $q = 50$ W/cm^2. In the figure, T_{0e} and T_{0p} are the electron and phonon temperatures at the cold end of the thermoelectric element (i.e., the interface between the vacuum gap and the thermoelectric element) respectively, and T_1 is the cooling target temperature. Two most distinctive features of this figure are: (1) The phonon temperature T_{0p} at the cold end is much higher than the electron temperature T_{0e}. The phonon temperature at the cold end can be even higher than the hot end temperature T_2 but the electrons at the cold end are still colder than T_2. This is because the Peltier effect cools the electrons first. (2) By using surface-plasmon coupling, the cooling target

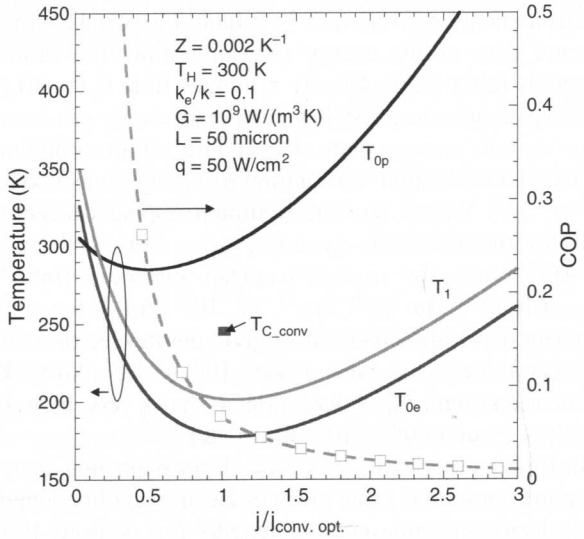

Fig. 7. Typical temperature and COP change with the applied current under a cooling load. T_{0e} and T_{0p} are the electron and phonon temperatures at the cold end of the thermoelectric element (i.e., the interface between the vacuum gap and the thermoelectric device) respectively, and T_1 is the cooling target temperature. Comparing to the minimum temperature $T = 250$ K that the conventional refrigerator can reach at such a cooling load at its optimum current density $j_{\text{conv. opt.}}$, the surface-plasmon coupled nonequilibrium thermoelectric refrigerator can reach a much lower temperature.

can reach as low as the electron temperature at the cold end. However, due to the additional thermal resistance or temperature drop at the vacuum side, the cooling target temperature T_1 is always higher than T_{0e} when there is an external cooling load. In this figure the cooling load is first calculated from the maximum cooling power density of a conventional thermoelectric refrigerator operating at $T_2 = 300$ K and $T_1 = 250$ K, which is $q = 50$ W/cm^2 for $L = 50$ μm device. Then such a cooling load is applied to the surface-plasmon coupled device to calculate the temperature distribution inside the device and the cooling target temperature by sweeping the applied current. As shown in the figure, compared to the minimum temperature $T = 250$ K that the conventional refrigerator can reach at such a cooling load at its optimum current $j_{conv.opt.}$, surface-plasmon coupled nonequilibrium thermoelectric refrigerator can reach much lower temperature. The minimum temperature with a cooling load of $q = 50$ W/cm^2 surface-plasmon coupled nonequilibrium thermoelectric refrigerator can achieve is $T_1 = 201.63$ K, which corresponds to $Z = 0.00547$ K^{-1} or $ZT_H = 1.641$ ($T_H = 300$ K). If the cooling target is kept at $T_1 = 250$ K, a much smaller current than the conventional optimum current $j_{conv.opt.}$ can be applied and thus a much higher COP, as large as 0.40, than the 0.092 of the conventional refrigerator can be achieved.

When the cooling load is removed, a thermoelectric refrigerator achieves its minimum temperature if the optimum current is applied. In a surface-plasmon coupled nonequilibrium thermoelectric refrigerator, this means that the cooling target temperature (both electrons and phonons at the cooling target) achieves the same temperature as the cold end electron temperature of the thermoelectric element. Figure 8(a) shows the minimum temperature of the surface-plasmon coupled nonequilibrium thermoelectric refrigerator as a function of thermoelectric element length for various G values. Apparently the shorter the thermoelectric element length and the smaller the coupling constant G, the lower the minimum temperature can be reached. Interestingly, for same $k_e/k = 0.1$, the minimum temperature can be grouped as function of dimensionless parameter GL^2/k. Figure 8(b) shows the minimum temperature as a function of GL^2/k for various k_e/k. For given values of Z and GL^2/k, the lower the k_e/k ratio, the lower the minimum temperature, which means the phonon heat flux has been cut off more effectively. Figure 9 shows the temperature distribution inside a 50 μm nonequilibrium thermoelectric refrigerator when the minimum cold end temperature is reached. The smaller the electron phonon coupling constant G, the larger the temperature difference between electrons and phonons. For small G values [10^8 and 10^{10} W/(m^3 K)], the electron temperature near the hot end can be larger than the phonon temperature but electrons are much colder than phonons at the cold side.

Figure 10 shows the performance of a surface-plasmon coupled nonequilibrium thermoelectric refrigerator under a

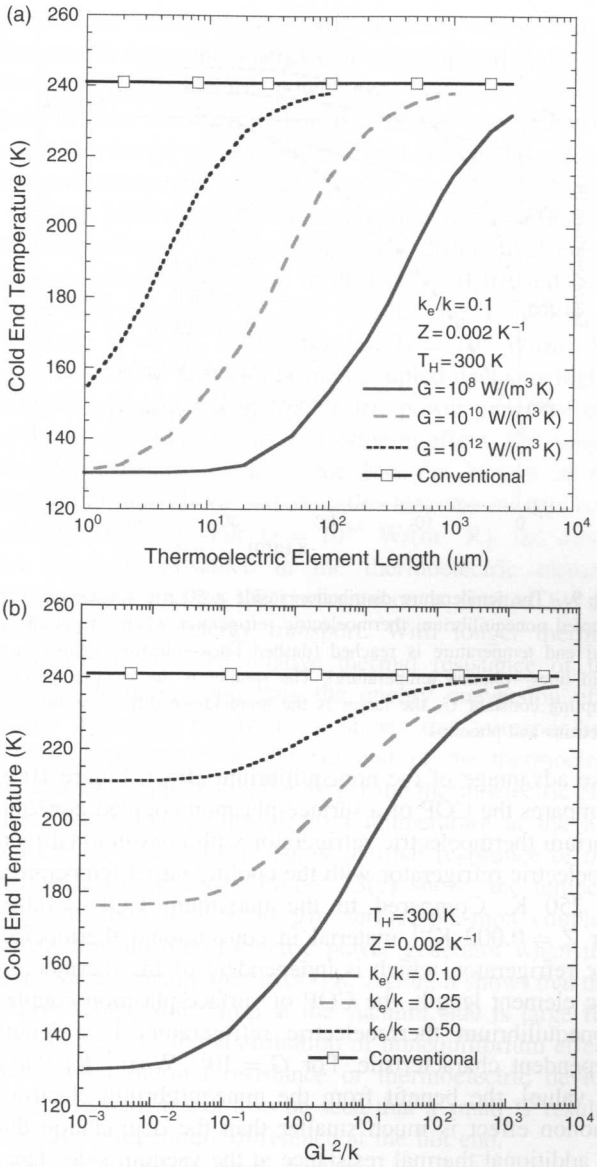

Fig. 8. (a) The minimum cooling temperature of the surface-plasmon coupled nonequilibrium thermoelectric refrigerator as a function of thermoelectric element length for various G values. The shorter the thermoelectric element length and the smaller the coupling constant G, the lower the minimum temperature can be reached. (b) the minimum temperature as a function of GL^2/k for various k_e/k.

cooling load of 50 W/cm^2, which is same as the maximum cooling power density of a $L = 50$ μm conventional thermoelectric refrigerator with $Z = 0.002$ K^{-1} operating at $T_H = 300$ K and $T_C = 250$ K. Figure 10(a) shows the cooling target temperature change with thermoelectric element length and the electron–phonon coupling constant. Also shown in the figure is the cooling target temperature for conventional thermoelectric refrigerators. Clearly, much lower cooling target temperature can be obtained for a wide range of G and L combinations than the conventional device with a same given load. For large G value, a smaller thermoelectric element length is necessary to

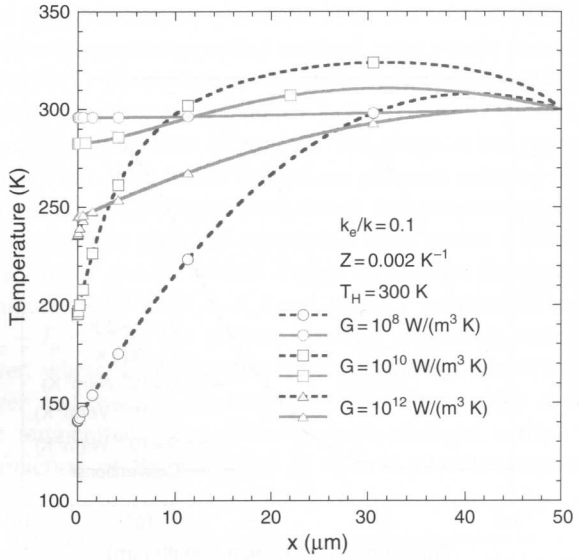

Fig. 9. The temperature distribution inside a 50 μm surface-plasmon coupled nonequilibrium thermoelectric refrigerator when the minimum cold end temperature is reached (dashed lines—electron temperature, solid lines—phonon temperature). The smaller is the electron phonon coupling constant G, the larger is the temperature difference between electrons and phonons.

take advantage of the nonequilibrium effect. Figure 10(b) compares the COP of a surface-plasmon coupled nonequilibrium thermoelectric refrigerator with conventional thermoelectric refrigerator with the cooling target temperature at 250 K. Compared to the maximum COP = 0.092 for $Z = 0.002\ K^{-1}$ material in conventional thermoelectric refrigerator, which is independent of the thermoelectric element length, the COP of surface-plasmon coupled nonequilibrium thermoelectric refrigerators is a length dependent characteristic. For $G = 10^{12}$ W/(m^3 K) [large G value], the benefit from the nonequilibrium electron–phonon effect is much smaller than the degradation due to additional thermal resistance at the vacuum side. Thus, the COP is always smaller than the conventional thermoelectric refrigerator. For low G values, the COP of surface-plasmon coupled nonequilibrium thermoelectric refrigerator can be much higher than the maximum of the conventional thermoelectric refrigerator.

As discussed in Section 2.2, there is small amount of energy flux due to the surface phonon polariton (the smaller peak in Fig. 4). The energy exchange through surface phonon polariton will degrade the performance calculated before since, in the case of refrigeration, the high phonon temperature in the thermoelectric element will cause a reverse flow of heat from the thermoelectric element to the cooling target. We have calculated the degradation caused due to this surface phonon polariton energy exchange. This is done by separating the energy exchange through surface plasmons and surface phonon polaritons. The boundary conditions (10) and (11) are changed accordingly. Figure 11 shows the cooling target temperature under a cooling load of 50 W/cm^2 with

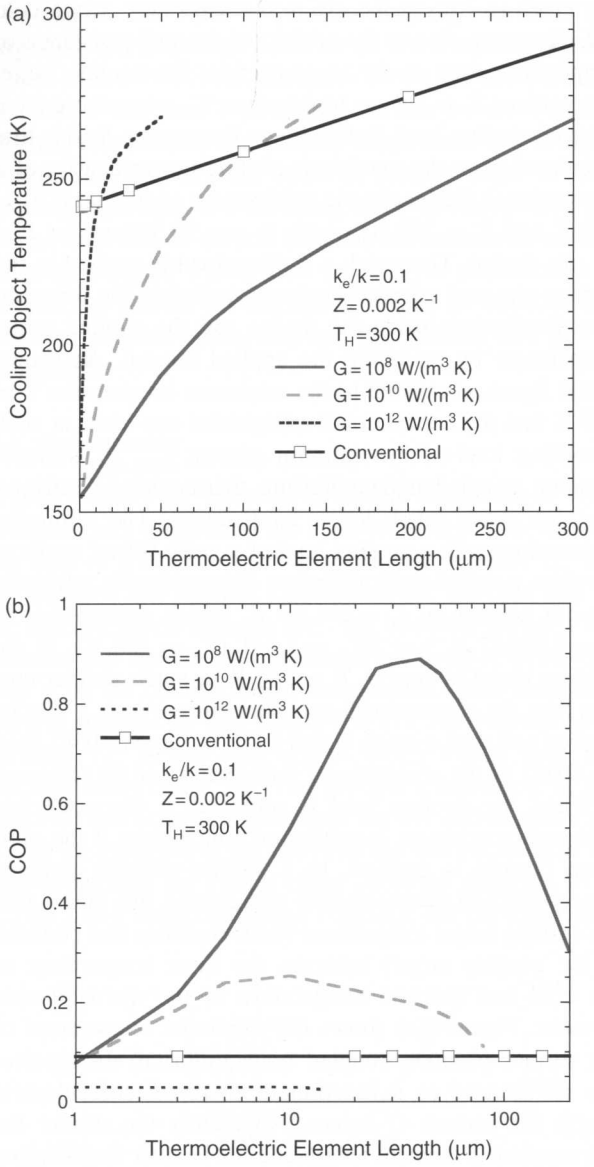

Fig. 10. (a) The cooling target temperature changes with thermoelectric element length and the electron–phonon coupling constant under a load of $q = 50$ W/cm^2. (b) The COP of surface-plasmon coupled nonequilibrium thermoelectric refrigerator as a function of thermoelectric element length and electron–phonon coupling constant with the cooling target temperature at 250 K. For low G value, the COP of surface-plasmon coupled nonequilibrium thermoelectric refrigerator can be much higher than the maximum of the conventional thermoelectric refrigerator.

(dashed lines) and without (solid lines) consideration of the degradation. The degradation can be a few degrees for short thermoelectric elements. However, the overall performance is still much better than the conventional thermoelectric refrigerator.

3.2. Power Generator

Figure 12 shows the typical change of the output power density and the energy conversion efficiency with the ratio of the external and internal thermal resistances

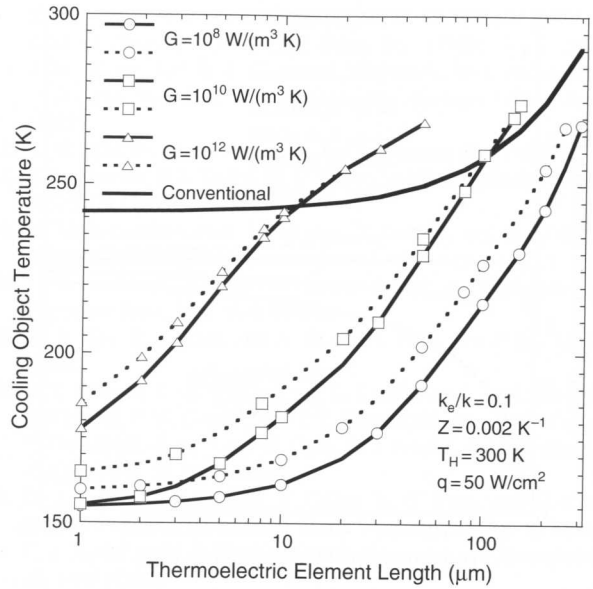

Fig. 11. The cooling target temperature with and without the consideration of the reverse energy flow due to surface phonon polariton (dashed lines with symbols–without, solid lines with symbols–with) under a cooling load of 50 W/cm^2. Though the surface phonon polariton degrades the cooling performance, the surface-plasmon coupled nonequilibrium devices have much better performance than conventional devices.

$\mu = R_L/R_{TE}$ operating with heat source temperature at 500 K and the cold side temperature at 300 K. Compared to the conventional thermoelectric power generator, the surface-plasmon coupled device has a much higher energy conversion efficiency over a wide range of $\mu = R_L/R_{TE}$. The optimum efficiency is around 1.5 times the optimum of conventional thermoelectric power generator for given

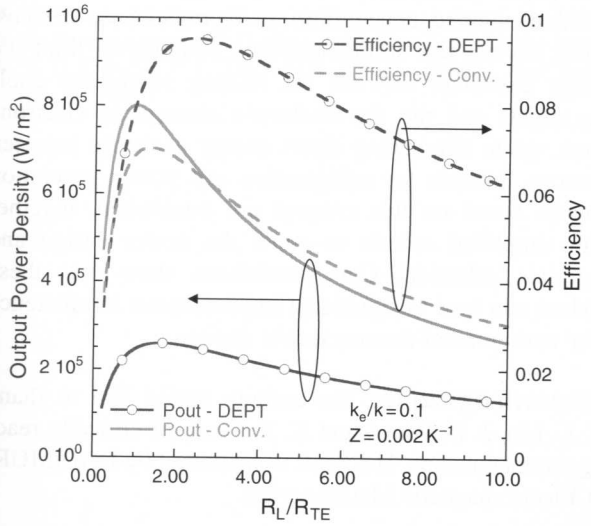

Fig. 12. Typical change of the output power density and the energy conversion efficiency with the ratio of the external and internal thermal resistances $\mu = R_L/R_{TE}$. Comparing to the conventional thermoelectric power generator, the surface-plasmon coupled nonequilibrium thermoelectric power generator has a much higher energy conversion efficiency over a wide range of $\mu = R_L/R_{TE}$.

parameters. However the high efficiency comes with a decrease in the output energy density compared to the conventional thermoelectric power generator. The efficiency gain is more of interest than the loss of energy density since the device power density must match the external thermal management capabilities.

Figure 13(a) shows the optimum efficiency as a function of thermoelectric element length for different electron–phonon coupling constant with $k_e/k = 0.10$ and $Z = 0.002$ K^{-1} operating at $T_1 = 500$ K and $T_2 = 300$ K. For both $G = 10^8$ W/(m^3 K) and $G = 10^9$ W/(m^3 K), the efficiency of surface-plasmon coupled device is higher than the conventional thermoelectric power generator due to the nonequilibrium electron–phonon effect. The longer the thermoelectric element, the less the benefit of the nonequilibrium effect and thus the less the energy conversion efficiency. For $G = 10^{12}$ W/(m^3 K), the effective thermal resistance in the thermoelectric element side is small and so the performance is limited by the surface-plasmon energy transport. With longer thermoelectric elements, the relative thermal resistance of the vacuum decreases and thus the energy conversion efficiency increases. Figure 13(b) shows the corresponding electron temperature at the hot end of the thermoelectric element. Apparently, the longer the thermoelectric element, the higher is the electron temperature at the hot end due to the relatively larger thermal resistance of the thermoelectric element. Figure 13(c) shows the temperature distribution in a 50 μm surface-plasmon coupled nonequilibrium thermoelectric power generator when the heat source is maintained at 500 K. Again, it shows that the relative temperature drop at the vacuum side is large for large G because the contribution of nonequilibrium effect to the total thermal resistance of thermoelectric device becomes small. It can also be seen that a small G results in a large temperature difference at the hot end.

Similar to refrigerator, the ratio of electron thermal conductivity contribution to the total thermal conductivity k_e/k also plays an important role in the energy conversion efficiency. Figure 14 shows the energy conversion efficiency as a function of thermoelectric element length for different k_e/k. It is interesting to see that increasing k_e/k results in a change of the device from nonequilibrium effect dominated regime ($k_e/k = 0.10$) to vacuum thermal resistance regime ($k_e/k = 0.50$) and results in a conversion energy decrease.

Comparing the performance calculation of refrigerators and power generators, we expect that the nonequilibrium transport favors the realization of refrigerators than power generators due to: (1) at low temperatures, the electron–phonon coupling constant G is several orders smaller; (2) at low temperatures, the thermal wavelength is longer and thus the vacuum gap can be larger. Finally we note that our calculation results shown above are not optimized. Though ZT is a good indicator for the performance of conventional thermoelectric devices, it is only one of the determining

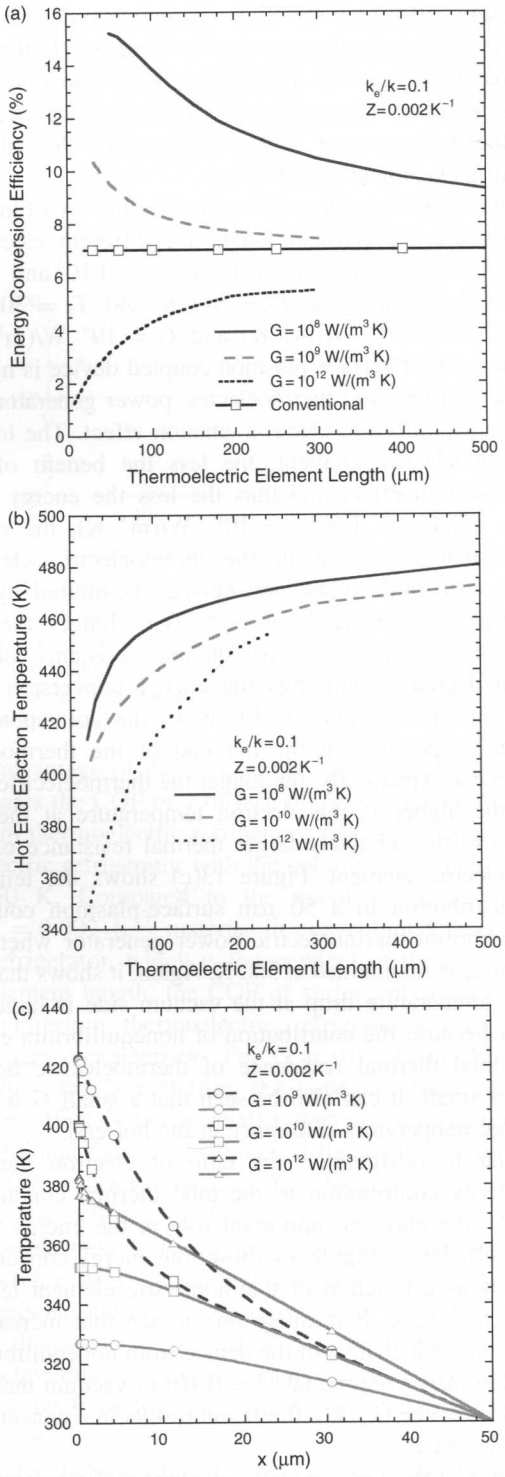

Fig. 13. (a) The optimum energy conversion efficiency as a function of thermoelectric element length for different electron–phonon coupling constant with $k_e/k = 0.10$ and $Z = 0.002$ K^{-1} operating at $T_1 = 500$ K and $T_2 = 300$ K, (b) The corresponding electron temperature at the hot end of the thermoelectric element. (c) The electron and phonon temperature distributions in a 50 μm surface-plasmon coupled nonequilibrium thermoelectric power generator when the heat source is maintained at 500 K.

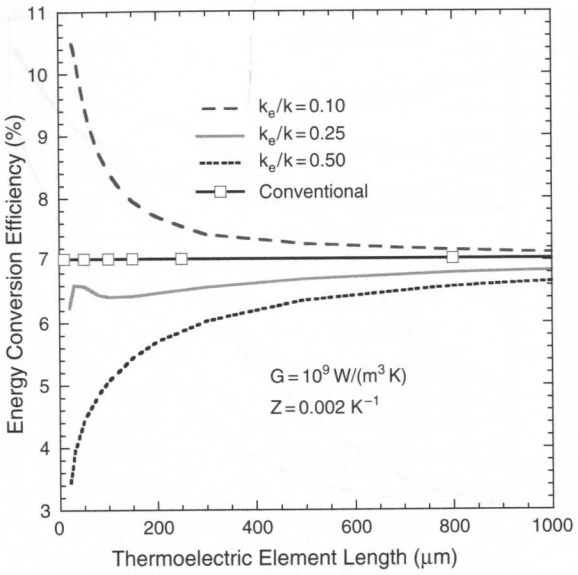

Fig. 14. The energy conversion efficiency changes as a function of thermoelectric element length for different k_e/k.

factors of the performance of the surface plasmon nonequilibrium thermoelectric devices. The optimum performance of such nonequilibrium devices are determined by the plasma frequency ω_p, and the damping γ_e, the electron–phonon coupling constant G, thermoelectric figure of merit ZT, and the contribution of the electrons to the total thermal conductivity, i.e., k_e/k. All these factors are strong functions of doping concentration and temperature. Optimization of such devices will be reported in the future.

4. CONCLUSIONS

This paper conceptualizes and investigates the surface-plasmon coupled nonequilibrium thermoelectric devices. These devices use surface-plasmon coupling to limit the energy exchange between the heating source (or cooling target) and the thermoelectric element to electrons alone, while eliminating direct energy exchange between phonons. Models for refrigeration and power generation devices based on this concept are established, together with simplified criteria to guide the device design and materials selection. Our simulations show that these devices can lead to significant improvements in efficiency over conventional thermoelectric devices.

Acknowledgments: The authors would like to thank W. L. Liu, J. B. Wang, and X. Y. Chen for critically reading the manuscript. The work is supported by DOD/MURI on Electromagnetic Metamaterials.

References

1. A. F. Ioff, *Semiconductor Thermoelements and Thermoelectric Cooling*, Info-search, London (**1956**); T. C. Harman and J. M. Honig, *Thermoelectric and Thermomagnetic Effects and Applications*, MacGraw-Hill, New York (**1967**); H. J. Goldsmid, *Electronic*

Refrigeration, Pion Ltd., London (**1986**); D. M. Rowe, *CRC Handbook of Thermoelectrics*, CRC Press, Inc. (**1995**); G. S. Nolas, J. W. Sharp, and H. J. Goldsmid, *Thermoelectrics: Basics Principles and New Materials Developments*, Springer-Verlag, Berlin (**2001**).

2. T. M. Tritt, Ed., *Semiconductors and Semimetals* 69–71 (**2001**).
3. T. C. Harman, P. J. Taylor, M. P. Walsh, and B. E. LaForge, *Science* 297, 2229 (**2002**).
4. R. Venkatasubramanian, E. Silvona, T. Colpitts, and B. O'Quinn, *Nature* 413, 597 (**2001**).
5. J. Tauc, *Photo and Thermoelectric Effects in Semiconductors*, Pergamon Press, New York (**1962**).
6. K. P. Pipe, R. J. Ram, and A. Shakouri, *Phys. Rev. B* 66, 125316 (**2002**).
7. B. J. O'Brien, C. S. Wallace, and K. Landecker, *J. Appl. Phys.* 27, 820 (**1956**); P. W. Cowling and J. E. Sunderland, *Energy Conversion* 7, 289 (**1968**); R. G. Yang, G. Chen, G. J. Snyder, and J.-P. Fleurial, *J. Appl. Phys.* 75, 8226 (**2004**).
8. G. J. Snyder, J.-P. Fleurial, T. Caillat, R. G. Yang, and G. Chen, *J. Appl. Phys.* 92, 1564 (**2002**); R. G. Yang, G. Chen, A. R. Kumar, G. J. Snyder, and J.-P. Fleurial, *Energy Conversion and Management*, 46, 1407 (**2005**).
9. A. Shakouri and J. E. Bowers, *Appl. Phys. Lett.* 71, 1234 (**1997**); G. D. Mahan and L. M Woods, *Phys. Rev. Lett.* 80, 4016 (**1998**).
10. C. B. Vining and G. D. Mahan, *J. Appl. Phys.* 86, 6852 (**1998**).
11. G. N. Hatsopoulos and J. Kaye, *J. Appl. Phys.* 29, 1124 (**1958**).
12. F. N. Huffman, U. S. Patent No. 3169200 (**1965**); Y. Hishinuma, T. H. Geballe, B. Y. Moyzhes, and T. W. Kenny, *J. Appl. Phys.* 94, 4690 (**2003**); *Appl. Phys. Lett.* 78, 2572 (**2001**).
13. T. J. Coutts, *Renewable Sustainable Energy Rev.* 3, 77 (**1999**).
14. V. S. Zakordonests and G. N. Logvinov, *Semiconductors* 31, 265 (**1997**); Yu G. Gurevich and G. N. Logvinoz, *Sov. Phys. Semicond.* 26, 1091 (**1992**).
15. Y. G. Gurevich and O. L. Mashkevich, *Phys. Rep. (Rev. Sec. Phys. Lett.)* 181, 327 (**1989**).
16. L. P. Bulat and V. G. Yatsyuk, *Sov. Phys.-Semicond.* 18, 383 (**1984**); L. I. Anatychuk, L. P. Bulat, D. D. Nikirsa, and V. G. Yatsyuk, *Sov. Phys.-Semicond.* 21, 206 (**1987**).
17. L. P. Bullat, Thermoelectricity under large temperature gradients. *J. Themoelect.* 4, 3 (**1997**).
18. G. Chen and T. Zeng, *Microscale Thermophyis. Eng.* 5, 71 (**2001**).
19. A. Narayanaswamy and G. Chen, *Appl. Phys. Lett.* 83, 3544 (**2003**).
20. E. G. Cravalho, C. L. Tien, and R. P. Caren, *ASME J. Heat Transf.* 89, 351 (**1967**).
21. D. Polder and M. Van Hove, *Phys. Rev. B* 4, 3303 (**1971**).
22. M. D. Whale, *A Fluctuational Electrodynamic Analysis of Microscale Radiative Heat Transfer and the Design of Microscale Thermophotovoltaic Devices*, Ph. D. thesis, MIT, Cambridge (**1997**).
23. R. S. DiMatteo, P. Greiff, S. L. Finberg, K. Young-Waithe, H. K. H. Choy, M. M. Masaki, and C. G. Fonstad, *Appl. Phys. Lett.* 79, 1894 (**2001**).
24. R. Carminati and J.-J. Greffet, *Phys. Rev. Lett.* 82, 1660 (**1999**).
25. L. Tsang, J. A. Kong, and K. H. Ding, *Scattering of Electromagnetic Waves*, Wiley (**2000**).
26. S. M. Rytov, Y. A. Kravtsov, and V. I. Tatarski, *Principles of Statistical Radiophysics*, Springer, Berlin (**1987**), Vol. 3.
27. P. P. Paskov, *J. Appl. Phys.* 8, 1890 (**1997**).
28. E. M. Conwell, *High Field Transport in Semiconductors*, Academic press, New York & London (**1967**).
29. R. R. Alfano, Ed., *Semiconductor Probed by Ultrafast Laser Spectroscopy*, Academic Press, New York (**1984**).
30. L. Challis, Ed., *Electron–Phonon Interactions in Low Dimensional Structure*, Oxford University Press, Oxford (**2003**).
31. R. W. Schoenlein, W. Z. Lin, J. G. Fujimoto, and G. L. Easley, *Phys. Rev. Lett.* 58, 1680 (**1987**).
32. T. Q. Qiu, and C. L. Tien, *Trans. ASME, J. Heat Transf.* 115, 835 (**1993**).
33. C. Wood, *Rep. Prog. Phys.* 51, 459 (**1988**).
34. J. M. Ziman, *Electrons and Phonons*, Clarendon, Oxford (**1960**).
35. K. Seeger, *Semiconductor Physics*, 8th, Springer, New York (**2002**).
36. B. K. Ridley, *Quantum Processes in Semiconductors*, Oxford University Press, Oxford (**1999**).
37. D. K. Ferry, *Semiconductor Transport*, Taylor & Francis, New York (**2000**).
38. B. K. Ridley, *Rep. Prog. Phys.* 54, 169 (**1991**).
39. R. Bower, R. W. Ure, J. E. Bauerle, and A. J. Cornish, *J. Appl. Phys.* 30, 930 (**1959**).
40. J. O. Sofo, G. D. Mahan, and J. Baars, *J. Appl. Phys.* 76, 2249 (**1994**).
41. M. I. Kaganov, M. I. Lifshitz, and L. V. Tanatarov, *Sov. Phys. JETP* 4, 173 (**1957**); J. Fujimoto, J. M. Liu, E. P. Ippen, and N. Bloembergen, *Phys. Rev. Lett.* 53, 1837 (**1984**); H. E. Elsayed-Al, T. B. Norris, M. A. Pessot, and G. A. Mourou, *Phys. Rev. Lett.* 58, 1212 (**1987**); P. B. Allen, *Phys. Rev. Lett.* 59, 1460 (**1987**); R. H. M. Groeneveld, R. Sprik, and A. Lagendijk, *Phys. Rev. B* 51, 11433 (**1995**).

Received: 13 October 2004. Accepted: 20 October 2004.